Helicon propagation in semiconductors in a quantizing magnetic field

B. A. Aronzon and E. Z. Meĭlikhov

I. V. Kurchatov Institute of Atomic Energy
(Submitted February 5, 1974)
Zh. Eksp. Teor. Fiz. **67**, 277–286 (July 1974)

Results are presented of an experimental investigation of the propagation of helicons in n-InSb and n-InAs under quantum-limit conditions (magnetic field up to 250 kOe) and at temperatures between 1.5 and 78 °K and frequencies of 24 and 39 GHz. Alternation of regions of strong and weak helicon damping (the magnetic field is varied) is observed in degenerate n-InSb and n-InAs samples at helium temperatures. This phenomenon is ascribed to changes in the dependence of the transverse component σ_{xx} of the conductivity tensor (determined in these conditions on the basis of scattering by ionized impurities) on the magnetic field strength. The change is due to the lifting of the electron degeneracy by the strong magnetic field in the quantum limit. The positions of the boundaries of the regions of weak and strong helicon damping depend on the electron concentration, temperature, wave frequency, and sample size. The proposed physical model of the phenomenon and the calculations performed on its basis are in agreement with the experimental data.

INTRODUCTION

The study of galvanomagnetic properties is a powerful method of investigating the structure of the energy spectrum and of carrier scattering in metals and semiconductors[1]. Particular interest attaches to a study of these phenomena in a quantizing magnetic field, which changes both the energy spectrum and the carrier-scattering mechanism. The greatest amount of information was obtained to date from measurements of the magnetoresistance (transverse and longitudinal) in a quantizing magnetic field. The value of this method is greatest when moderate (but quantizing) magnetic fields are used, which lead to the appearance of well-resolved oscillatory phenomena. In the quantum limit, which is of particular interest for a number of reasons, no such oscillations occur and the interpretation of the results of the galvanomagnetic measurements is frequently quite difficult, since the corresponding relations (for example, the dependence of the magnetoresistance on the magnetic field) are smooth and have no strongly pronounced singularities. It is difficult then to determine with sufficient accuracy the changes of the scattering mechanism or of the carrier statistics. Since, in addition, the magnetoresistance is determined also by the carrier density, additional difficulties arise when the density is a function of the magnetic field, (for example in semimetals and semiconductors). A major (although not principal) shortcoming of the traditional methods is the difficulty of obtaining exact results in pulsed magnetic fields, which frequently are the only ones available to the experimenters.

A method free of many of the foregoing shortcomings is the study of the propagation of weakly-damped electronmagnetic waves (helicons) in a solid-state plasma[2]. In this case one measures simultaneously (by determining the dispersion and the damping of the helicon) the Hall component (σ_{yx}) and the transverse component (σ_{xx}) of the conductivity tensor. This makes it possible to determine the density and scattering mechanism of the carriers. It is important that the damping of the helicon is an exponential function of the components of the conductivity tensor, and this makes it possible to determine more accurately (than in the magnetoresistance method) the change produced in σ_{xx} by the change in the character of the carrier scattering in the magnetic field. In addition, helicon damping is in essence a size-dependent effect, since its magnitude depends (exponentially) on the dimension of the system along the helicon propagation direction. Thus, we have an additional parameter, namely the sample dimension, and variation of this parameter enables us in principle to measure the function $\sigma_{xx}(H)$ more accurately.

The helicon method was used successfully for metals and semiconductors to measure the carrier density, to study quantum oscillations, cyclotron absorption, as well as other phenomena in an electron plasma of a solid[3]. It should be noted at the same time that systematic investigations of helicon propagation in the quantum limit were in fact not carried out, although the attainment of this regime (at least for semiconductors) does not entail great experimental difficulties. One of the many studies in this direction was carried out by Furdina[4], who observed a strong increase of helicon damping in the degenerate electron gas of n-InSb in the quantum limit at helium temperature. We have previously investigated[5] the dispersion of a helicon in n-InSb at nitrogen temperature in the presence of a change of the carrier density in the quantum limit. In[6], singularities were predicted in helicon propagation in the quantum limit, due to the influence of the magnetic field on the statistics and on the carrier scattering mechanism. In our recent paper[7], we described preliminary results of a study of these singularities in n-InSb at helium temperature in a magnetic field up to 250 kOe.

The present paper is devoted to a detailed exposition of the experimental data and to an analysis of the physical phenomena discussed in[6].

FEATURES OF HELICON PROPAGATION IN THE QUANTUM LIMIT

1. Let us examine briefly the ideas underlying the helicon method of investigating the conductivity tensor of a semiconductor in a quantizing magnetic field. The dispersion relation for a helicon propagating in a pure electronic along an external magnetic field is[3]

$$\frac{k^2c^2}{\omega^2}=\varkappa+\frac{4\pi}{\omega}\sigma_{yx}+i\frac{4\pi}{\omega}\sigma_{xx}. \tag{1}$$

Here ω and k are the frequency and wave vector of the wave, while κ is the static dielectric constant of the crystal.

In the customarily considered case $\sigma_{xx} \ll \sigma_{yx}$, the spatial damping of the helicon, determined by the imaginary part of the wave vector, is small. The expressions for $k_r = \mathrm{Re}\, k$ and $k_i = \mathrm{Im}\, k$ take in this case the form

$$k_r = \frac{(4\pi\omega\sigma_{yx}')^{1/2}}{c}, \quad k_i = \frac{1}{2} k_r \frac{\sigma_{xx}}{\sigma_{yx}'} \ll k_r, \tag{2}$$

where $\sigma_{yx}' = \sigma_{yx} + \kappa\omega/4\pi$. In the general case (at an arbitrary ratio of σ_{xx} and σ_{yx}), the corresponding expressions become more complicated:

$$k_r = \frac{(4\pi\omega\sigma_{yx}')^{1/2}}{c} \varphi_r\left(\frac{\sigma_{xx}}{\sigma_{yx}'}\right), \quad k_i = \frac{1}{2} k_r \frac{\sigma_{xx}}{\sigma_{yx}'} \varphi_i\left(\frac{\sigma_{xx}}{\sigma_{yx}'}\right). \tag{3}$$

Here

$$\varphi_r(u) = \frac{1}{\sqrt{2}}[(1+u^2)^{1/2}+1]^{1/2}, \quad \varphi_i(u) = \frac{2}{u^2}[(1+u^2)^{1/2}-1]. \tag{4}$$

Direct calculations show that at $u \leq 1$ the values of the functions $\varphi_r(u)$ and $\varphi_i(u)$ differ from unity by not more than 10 and 20%, respectively. This means that in the case $\sigma_{xx} \leq \sigma_{yx}$ (and it is precisely this case which will be of interest to us in the future) it is possible, subject to the indicated error, to use the simple relations (2), according to which the dispersion of the helicon is determined by the Hall conductivity σ_{yx} and its damping is determined by the dissipative (transverse) conductivity σ_{xx}.

We define the transparency coefficient β of a helicon passing through a sample of thickness L as the ratio of the amplitude of the field incident on the sample to the waves passing through it. Then, under the conditions $k_r L \gg k_i L \gg 1$, we have[3]

$$\beta = \beta_r \exp(-k_i L) \cong \beta_r \exp\left(-\frac{1}{2} k_r \frac{\sigma_{xx}}{\sigma_{yx}'} L\right),$$
$$\beta_r = \frac{4ck_r/\omega}{(ck_r/\omega+1)^2} \exp(ik_r L). \tag{5}$$

According to (5), the transparency coefficient is a complicated function of the magnetic field, defined by the dependences of the conductivity tensor components $\sigma_{xx}(H)$ and $\sigma_{yx}'(H)$ on the magnetic field. To determine the approximate form of this function, we note that in a strong (including quantizing) magnetic field we have $\sigma_{yx} = nec/H$[8], and $\sigma_{xx}(H)$ has a complicated form determined by the statistics and the mechanism of the electron scattering.

2. We continue the analysis by using as an example a degenerate (at H = 0) n-type semiconductor, in which the electrons are scattered by ionized impurities at sufficiently low temperatures. In this case there are at least four regions of values of the strong magnetic field, which differ significantly in the form of the $\sigma_{xx}(H)$ dependence[1)].

1) Classical magnetic field ($\Omega\tau \gg 1$, $\hbar\Omega \ll \epsilon_F$); in this case

$$\sigma_{xx} \propto 1/\Omega^2 \tag{6}$$

2) Quantizing magnetic field ($\Omega\tau \gg 1$, $\hbar\Omega \lesssim \epsilon_F$); region of quantum oscillations; σ_{xx} oscillates when the magnetic field is varied.

3) Quantum limit, degenerate electrons ($0 < \epsilon_F - \frac{1}{2}\hbar\Omega < \hbar\Omega$); in this case[8]

$$\sigma_{xx} \propto \Omega. \tag{7}$$

4) Quantum limit, electron degeneracy lifted by the magnetic field ($\epsilon_F - \frac{1}{2}\hbar\Omega < 0$); in this case[7]

$$\sigma_{xx} \propto \frac{1}{\Omega^2}. \tag{8}$$

We shall be interested mainly in the last two regions of the magnetic field—the quantum limit.

Figure 1 shows plots of $\sigma_{xx}(H)$, $\sigma_{yx}'(H)$, and $\beta(H)$ for an n-InSb sample at T = 4.2°K with electron density (at H = 0) $n_0 = 10^{16}$ cm^{-3}. The function $\sigma_{xx}(H)$ for this case was calculated with the aid of Neuringer's experimental data[9] on the magnetoresistance and the Hall effect. The frequency $\omega = 2 \times 10^{11}$ sec^{-1} corresponds to the 8-mm wavelength band, and L = 4.2 mm. This figure reveals the existence of a region where the magnetic field is not transparent to the helicon; this region lies in the field interval $H_1 < H < H_2$; the lower limit of this region is connected with the growing function $\sigma_{xx}(H)$ in the quantum limit for degenerate electrons (relation (7)), while the upper limit is connected with the decreasing function $\sigma_{xx}(H)$ in the quantum limit after the electron degeneracy is lifted by the magnetic field (relation (8)). Like any other characteristic quantity connected with an exponential dependence (for example, the dimension of the skin layer, the relaxation times, etc.), the limiting values H_1 and H_2 are defined quite arbitrarily. We define them as those values of the magnetic field at which the transparency coefficient becomes smaller by a factor e^2 than its maximum value (for fields $H < H_1$), meaning $\beta(H_{1,2}) = e^{-2}\beta_{max}$. This definition was used to estimate the values of H_1 and H_2 in Fig. 1. All the experimental and calculated values of H_1 and H_2 cited below are based on this definition.

It is clear from physical considerations that the limits of the non-transparency region should lie respectively inside the field regions $H_{qu.lim.} < H_1 < H_{deg}$ and $H_2 > H_{deg}$ ($H_{qu.lim}$ is the field at which the quantum limit sets in, and H_{deg} is the field at which the degeneracy is lifted). We estimate $H_{qu.lim}$ and H_{deg} with the aid of the expression

$$n(H) = \frac{N_c}{2\sqrt{\pi}} \frac{\hbar\Omega}{k_0 T} F_{-1/2}\left[\frac{\epsilon_F - {}^1/_2\hbar\Omega + G\hbar\Omega}{k_0 T}\right],$$
$$N_c = \frac{(2\pi m^* k_0 T)^{3/2}}{4\pi^3\hbar^3}, \quad G = \frac{1}{4}\frac{m^*}{m_0}|g^*|, \tag{9}$$

which connects the concentration and the Fermi energy of the electrons in the quantum limit;

$$F_{-1/2}(x) = \int_0^\infty \frac{t^{-1/2}\,dt}{1+\exp(t-x)},$$

g^* is the effective Landé factor for electrons. We put $\epsilon_F = \hbar\Omega/2$, which corresponds to placing the Fermi level halfway between the two lower (spin-split) Landau sublevels. It follows then from (9) (with allowance for the asymptotic relation $F_{-1/2}(x) \cong 2\sqrt{x}$ at $x \gg 1$ and under the condition $n - n_0$) that

$$\hbar\Omega_{\text{qu. lim.}} = \epsilon_{F0}(4/3\sqrt{G})^{2/3}. \tag{10}$$

Here n_0 and ϵ_{F0} are the concentration and the Fermi

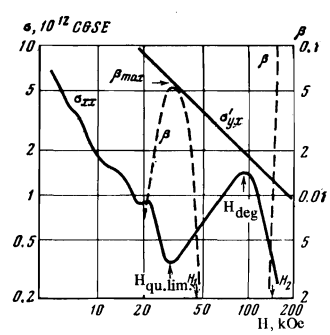

FIG. 1. Dependence of the conductivity-tensor components σ_{xx} and σ_{yx}' and of the transparency coefficient β on the magnetic field for n-InSb with electron density $n_0 = 10^{16}$ cm^{-3} at T = 4.2° K; σ_{xx} is plotted from the data of [9], and β is calculated for L = 4.2 mm. The plot of σ_{yx}' was constructed without allowance for the magnetic quenching, which is significantly cancelled out by the contribution of κ.

energy of the electron at H = 0. The value of the magnetic field H_{deg} is obtained by assuming (arbitrarily) that $(\epsilon_F - \hbar\Omega/2 + G\hbar\Omega)/k_0T = 1.1$ (this corresponds to the inflection point of the function $F_{-1/2}$). We then obtain from (9) the relation

$$\hbar\Omega_{deg} = k_0 T \frac{2\sqrt{\pi}}{F_{-1/2}(1,1)} \frac{n(\Omega_{deg})}{N_c}, \qquad (11)$$

in which we took into account the dependence of the electron density on the magnetic field as a result of the "magnetic quenching" effect, which is connected with the lifting of the electron degeneracy. We note that in accordance with (10) and (11) we have

$$H_{qu.\,lim.} \propto T^0, \quad H_{deg} \propto T^{-1/2}.$$

EXPERIMENTAL PROCEDURE

To study helicon propagation in n-InSb and n-InAs at the frequency 39 GHz, we used the two-beam interferometer system shown in Fig. 2. Microwave radiation from a klystrom generator K entered both channels of the waveguide system; part of the microwave power propagated through a waveguide placed in a Dewar vessel and passed through the sample, which was placed in this waveguide. To prevent "leakage" of the signal past the sample, the transverse dimensions of the sample were made to match exactly the dimensions of the waveguide, and the sample was glued into a plastic plate (with adhesive that absorbed microwave radiation) clamped between the flanges of the waveguide (see Fig. 2). The second arm of the waveguide system included an attenuator (A) and a phase shifter (Ph). The signal, the result of the interference of the reference and investigated signals, was measured with a detector (D). Thus, the experimental setup is in fact a Rayleigh interferometer[2], and the extrema of the interference pattern produced by the variation of the wave vector of the wave in the sample ($k_r = k_r(H)$) are given by the relation $k_rL = M\pi$, where $M = 1, 2, 3, \ldots$, L is the sample thickness. By measuring the phase of the reference signal (it is necessary in this case to monitor the constancy of the amplitude of the reference signal), one can obtain a series of interference patterns, the envelope of which determines the dependence of the power passing through the sample on the value of the magnetic field. From these dependences it is possible to determine the limiting fields H_1 and H_2 by the method described above (the accuracy with which H_1 and H_2 are determined is ~10%).

The measurements were performed in pulsed magnetic fields up to 250 kOe in the temperature range 1.5–100°K. The samples were prepared by the standard procedure and their parameters are listed in Table I.

EXPERIMENTAL RESULTS AND DISCUSSIONS

Typical experimental results are shown, in the form of interference patterns, in Fig. 3 for sample 815 S. The interference pattern 2, which corresponds to helicon propagation at T = 12.2°K, differs strongly from interference pattern 1, which is obtained at T = 78°K. The helicon attenuates strongly in the region $H_1 < H < H_2$.

Table II shows the experimental values of the limiting fields H_{1e} and H_{2e} for different samples. The table shows also that the values of $H_{qu.lim}$ and H_{deg} calculated with the aid of (10) and (11). It lists also the calculated values of H_{1c} and H_{2c} obtained by the method described above.

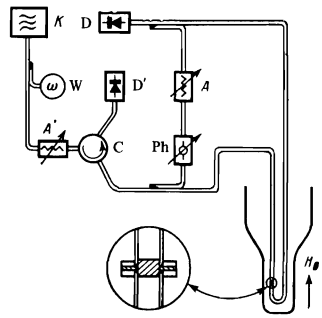

FIG. 2. Experimental setup: K–klystron microwave generator, W–wavemeter, A, A'–attenuators, D, D'–detectors for the transmitted and reflected waves, C-circulator, Ph–phase shifter. The mounting of the sample is shown in the insert.

TABLE I

Sample No.	Material	n_0, cm^{-3}	μ*, cm^2/V-sec	L, mm
315S	n-InSb	$3.5\cdot10^{15}$	213 000	6
815S		$7.7\cdot10^{15}$	148 000	4.2 **
116S		$1\cdot10^{16}$	165 000	4.3
316S		$2.6\cdot10^{16}$	88 000	5
416S		$4\cdot10^{16}$	120 000	5.5
216A	n-InAs	$1.7\cdot10^{16}$	24 100	2.4

*μ–mobility at 77°K.
**The thickness of this sample was varied between 2 and 7.2 mm.

TABLE II

Sample No.	H, kOe					
	$H_{qu.\,lim.}$	$H_1 l$	H_{1c}	H_{deg}	$H_2 l$	H_{2c}
315S	11	19	22	30	38	41
815S	22	52	—	77	122	—
116S	25	54	46	100	126	140
316S	40	75	—	180	105	—
416S	55	115	—	330	>250	—
216A	51	95	—	120	110	—

As seen from Table II, the values of H_{1e} increase with increasing electron density. The reason is that the strong helicon damping, which begins in a field H_1, is due to the relation $\sigma_{xx} \propto H$, which holds true only in the quantum limit. On the other hand, the field $H_{qu.lim}$ at which the quantum limit sets in increases with increasing concentration (see (10) and Table II).

One should expect also an increase of the field H_2 with increasing n_0, since the field H_{deg} at which the degeneracy is lifted increases with increasing density (see (11) and Table II). The tendency of this growth is seen from the values of H_{2e} listed in Table II, although the ratio of the values of H_{2e} for the samples 116 S and 316 S does not agree with the expected value[3].

For sample 416 S we have H_{deg} = 330 kOe, which exceeds the field attained in the present experiments. We were therefore unable to observe in this sample the appearance of a second transparency region; it can only be stated that $H_2 > 250$ kOe in this case.

It is seen from Table II that the calculated values H_{1c} and H_{2c} are in satisfactory agreement with the experimental values H_{1e} and H_{2e} for those samples for which this calculation could be performed from data on the magnetoresistance and on the Hall effect (see the curves of Fig. 1, which were plotted in accordance with the experimental data[9]).

Figure 4 shows a series of interference patterns for n-InSb samples with identical density $n_0 = 7.7 \times 10^{15}$ cm^{-3} and with different thicknesses (2, 3, 3.5, 4.2, and 7.2 mm). It is seen from this figure that when the sam-

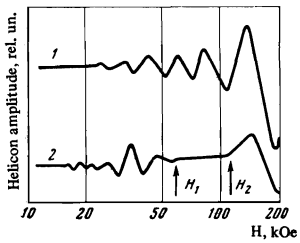

FIG. 3

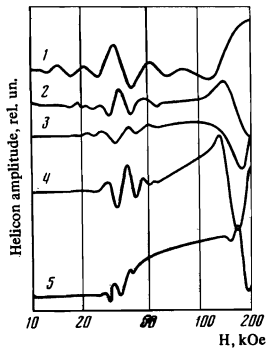

FIG. 4

FIG. 3. Interference patterns for sample 815 S (Rayleigh interferometer): 1–78° K, 2–4.2° K.

FIG. 4. Interference patterns for n-InSb samples with electron density $n_0 = 7.7 \times 10^{15}$ cm^{-3} and with different thicknesses L at T = 4.2° K (Rayleigh interferometer): 1–2, 2–3, 3–3.5, 4–4.2, 5–7.2 mm.

ple thickness is decreased the non-transparency region decreases gradually and vanishes completely at L = 2 mm. The narrowing of the non-transparency region with decreasing sample thickness is due to the fact that the transparency coefficient β depends on the sample thickness (see (5)). Let $k_{i\,max}$ be the value of k_i at the maximum transmission point; then the values of the magnetic field H_1 and H_2 are determined by the equation $k_i(H_{1,2}) = k_{i\,max} + 2/L$, where the function $k_i(H)$ has a maximum at $H \cong H_{deg}$. It is therefore clear that a decrease of L should bring the values of H_1 and H_2 closer together, i.e., it should cause the non-transparency region to become narrower, as is indeed observed in the experiment.

It is clear from (2) and (5) that a change in the frequency of the incident wave should generally speaking influence the values of the fields H_1 and H_2 in analogy with a change in the sample thickness L, i.e., a decrease of the frequency should make the non-transparency region narrower. This was confirmed by an experiment on the sample 815 S with thickness L = 3 mm, for which the measured values of the fields H_1 and H_2 amount to 69 and 100 kOe at 24 GHz, as against 59 and 110 kOe at 39 GHz.

Under the conditions

$$\frac{4\pi}{\omega}\sigma_{yx} = \frac{4\pi nec}{\omega H} \gg \varkappa, \quad \sigma_{yx} > \sigma_{xx}$$

the relation $k_r L = M$ (M is the number of the extremum of the interference pattern), which determines the positions of the extrema of the interference pattern, takes the form

$$M = \left(\frac{4ne\omega L^2}{\pi c}\right)^{1/2} \frac{1}{\sqrt{H}}. \qquad (12)$$

It follows therefore that a plot of $M(H^{-1/2})$ should be a straight line (assuming that n is constant), the slope of which depends on the electron density. Figure 5 shows the corresponding plots for a sample with electron density $n_0 = 7.7 \times 10^{15}$ (L = 2 mm) at temperatures 4.2 and 78°K. It is seen that in strong magnetic fields the experimental points deviate from a straight line, and this deviation has different signs for helium and nitrogen temperatures.

At T = 78°K, the noted deviation is connected with two factors that "work" in the same direction—the contribution of $\varkappa$ to the dispersion relation (1) and the in-

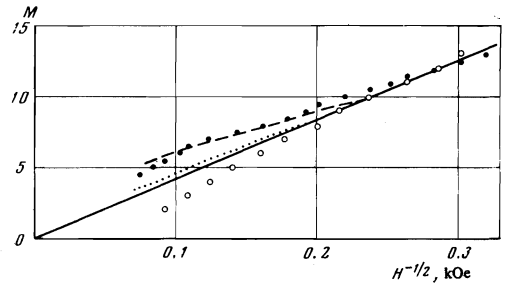

FIG. 5. Plots of $M(H^{-1/2})$ for the sample n-InSb with electron density $n_0 = 7.7 \times 10^{15}$ cm^{-3} (L = 2 mm): ●–T = 77°K, Fabry-Perot interferometer; ○–T = 4.2°K, Rayleigh interferometer. The straight line corresponds to the relation $M = 4(n_0 e\omega L^2/\pi c)^{1/2} H^{-1/2}$, and the dotted line is a plot of formula (1) with $\varkappa$ taken into account, while the dashed line is calculated with allowance for $\varkappa$ and for the change of the electron density in the magnetic field (in accordance with [10]).

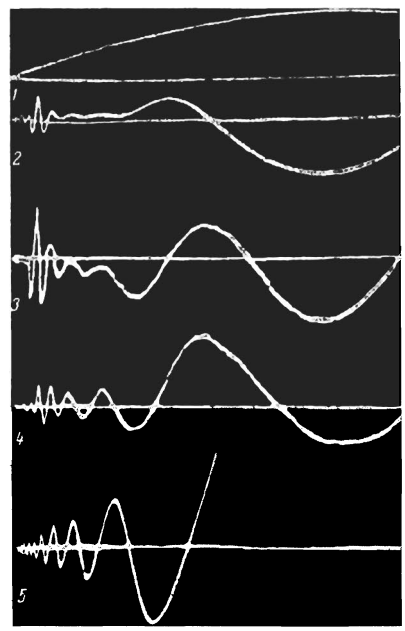

FIG. 6. Interference patterns for sample 315 S at different temperature (Rayleigh interferometer): 1–time scan of magnetic field (maximum of value 200 kOe); 2–4.2°; 3–10°, 4–17°; 5–35° K. The sensitivity of the measurement circuit in the case of oscillogram 2 is half as large as in the case of oscillograms 3–5.

crease of the electron density in a strong magnetic field[10]. The latter factor is particularly clearly manifest in samples with lower electron density (samples 315 S and 815 S), inasmuch as at high density the overlap of the conduction and impurity bands prevent the electron density from increasing with increasing magnetic field. Figure 5 shows also theoretical plots of $M(H^{-1/2})$ with this effect taken into account. A qualitative agreement between experiment and theory is seen.

At T = 4.2°K, the experimental plot of $M(H^{-1/2})$ deviates from a straight line in a direction corresponding to a decrease of the electron density, this being connected with the "magnetic quenching" of the electrons.

It was indicated above that the value of the field H_1 should not depend (in degenerate samples) on the temperature, and that the field H_2 should increase with decreasing T, inasmuch as $H_2 > H_{deg} \propto T^{-1/2}$ (without allowance for the effect of "magnetic quenching," see (11)). Measurements carried out at T = 1.5°K have shown that within the limits of the measurement ac-

curacy the value of H_1 remains unchanged (in comparison with the data obtained at $T = 4.2°K$), while H_1 increases by 11, 12, and 10 kOe respectively for the samples 315 S, 815 S, and 316 S. The increase is less than expected, this being attributed to an enhancement of the effect of "magnetic quenching" with decreasing temperature. It appears that the same effect is the cause of the vanishing of the non-transparency region (as defined by us) for the sample 216 A at $T = 1.5°K$.

A rise in temperature (above 4.2°K) leads to an appreciable decrease of H_2. Above a certain temperature, the degeneracy-lifting field becomes smaller than $H_1|_{T=4.2°K}$, and this leads to a vanishing of the non-transparency region for the helicon.

Figure 6 shows a series of interference patterns for sample 815 S at different temperatures. The gradual vanishing of the region of non-transparency with increasing temperature is clearly seen. An estimate of the temperature T_{cr} corresponding to the vanishing of this region can be obtained with the aid of the relation $H_{deg}(T_{cr}) = H_1|_{T=4.2°K}$, from which we obtain, with the aid of (11), $T_{cr} = 16°K$, in accord with the experimental data.

The authors are grateful to I. K. Kikoin for constant interest in the work and for a discussion of the results.

[1)] In relations (6)–(8), Ω is the electron cyclotron frequency, τ is the electron-momentum relaxation time, and ϵ_F is the Fermi energy.

[2)] In a number of cases, the measurements were performed also with the apparatus operating as a Fabry-Perot interferometer (this was done by eliminating the "reference" arm from the circuit of Fig. 2).

[3)] This may be due to the low mobility of the electrons in sample 316 S (see Table I).

[1] I. M. Lifshitz, M. Ya. Azbel', and M. I. Kaganov, Elektronnaya teoriya metallov (Electron Theory of Metals), Nauka (1971).
[2] B. F. Maxfield, Am. J. Phys. **37**, 241 (1969).
[3] E. D. Palik and J. K. Furdina, Rep. Progr. Phys., 33, 1193 (1970).
[4] J. K. Furdina, Phys. Rev. Lett., 16, 646 (1966).
[5] E. Z. Meĭlikhov and B. A. Aronzon, Dokl. Akad. Nauk SSSR 206, 1329 (1972) [Sov. Phys. Dokl.
[6] E. Z. Meilikhov, Fiz. Tekh. Poluprovodn. 6, 839 (1972) [Sov. Phys.-Semicond. 6, 726 (1972)].
[7] B. A. Arozon and E. Z. Meĭlikhov, ZhETF Pis. Red. 18, 400 (1973) [JETP Lett. 18, 235 (1973)].
[8] E. N. Adams and T. D. Holstein, J. Phys. Chem. Sol., 1, 137 (1956).
[9] L. J. Neuringer, in: Trudy IX Mezhdunarodnoĭ konferentsii po fizike poluprovodnikov (Proc. 9th Internat. Conf. on Semiconductor Physics), Nauka, Vol. 2 (1969), p. 757.
[10] B. A. Aronzon and E. Z. Meĭlikhov, Zh. Eksp. Teor. Fiz. 61, 1906 (1971) [Sov. Phys.-JETP 34, 1014 (1972)].

Translated by J. G. Adashko
36